High-pressure single-crystal neutron diffraction to 10 GPa by angle-dispersive techniques

Journal of
Applied Crystallography

ISSN 0021-8898

Received 5 November 2010
Accepted 6 June 2011

High-pressure single-crystal neutron diffraction to 10 GPa by angle-dispersive techniques

Craig L. Bull,[a]* Malcolm Guthrie,[a]‡ John Archer,[b] Maria-Teresa Fernandez-Diaz,[b] John S. Loveday,[a] Kazuki Komatsu,[a]¶ Hayrullo Hamidov[a] and Richard J. Nelmes[a]

[a]SUPA, School of Physics and Astronomy and Centre for Science at Extreme Conditions, University of Edinburgh, Mayfield Road, Edinburgh EH9 3JZ, UK, and [b]Institut Laue–Langevin, BP156, 6 rue Jules Horowitz, 3042 Grenoble Cedex 9, France. Correspondence e-mail: craig.bull@stfc.ac.uk

Techniques have been developed that allow the measurement of accurate single-crystal neutron-diffraction data at pressures up to 10 GPa, using angle-dispersive methods. High-quality data have been collected up to 10 GPa, to a resolution of $\sin\theta/\lambda \simeq 1.5$ Å^{-1}, from samples of size 3–4 mm^3. This article presents the methods developed to mount and centre the sample accurately on the instrument; to reduce the background and hence increase the precision of the measured reflection intensities; and to increase further the accessible region of reciprocal space with a single sample loading. Developments are also highlighted, with a view to increasing the range of both science and pressures that can be achieved at the Institut Laue–Langevin reactor source using single-crystal techniques.

1. Introduction

For the determination of detailed structural information such as the accurate measurement of atomic displacement parameters or the resolution of multi-site disorder, single-crystal neutron diffraction is the technique of choice (McMahon *et al.*, 1990). However, the relatively large volumes required for neutron diffraction make single-crystal techniques difficult to use at high pressure (Bull, Guthrie, Nelmes, Loveday, Komatsu *et al.*, 2009), and, until recently, they have been limited to 2 GPa (Nelmes *et al.*, 1987; Kuhs *et al.*, 1989; Tun *et al.*, 1987). We have recently succeeded in reaching 10 GPa with time-of-flight methods (Bull, Guthrie, Nelmes, Loveday, Komatsu *et al.*, 2009), which offer some technical advantages in data collection. However, angle-dispersive techniques using a monochromatic neutron beam also have their advantages. In particular, it is possible to devote experimental time to measuring those reflections known (or shown in pre-scans) to be most readily measurable (*i.e.* strong enough) and also those that have the highest 'leverage', *i.e.* the ones that are most sensitive to the important features or parameters of the structure (Hazen & Finger, 1989). The use of monochromatic radiation greatly simplifies the correction for wavelength-dependent parameters such as incident-beam flux, detector efficiency and attenuation, permitting increased precision in structure refinement. In addition, background levels are generally lower for monochromatic beams on reactor sources, which do not have the intrinsically large gamma radiation and high-energy neutron backgrounds of spallation sources. In this paper, we describe techniques we have recently developed to perform room-temperature studies up to 10 GPa using the angle-dispersive single-crystal diffractometer, D9, at the Institut Laue–Langevin (ILL) in Grenoble, France.

2. D9 and single-crystal diffraction

Fig. 1 shows the layout of the D9 diffractometer. The instrument works in two modes of operation: either 'four-circle' or 'normal-beam' (lifting-counter) geometry. In four-circle geometry, the sample holder is an offset Eulerian cradle (χ circle). The instrument is positioned in the ILL reactor hall with a view of the graphite hot source. This is the only reactor source currently capable of providing neutrons with sufficient

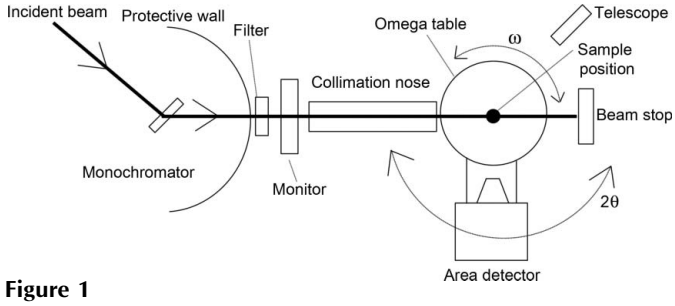

Figure 1
Schematic plan view of the layout and essential components of the D9 diffractometer at the ILL in 'normal beam' mode. The relative positions of components are shown around the neutron beam, starting at the left with the incident beam from the hot source impinging on the monochromator, through to the sample position and the detector and beam stop. The ω and 2θ angles of the sample and detector rotations are labelled. A more detailed description of key components is given in the text.

‡ Present address: Geophysical Laboratory, Carnegie Institution of Washington, Washington, DC 20015, USA.
¶ Present address: Geochemical Research Center, Graduate School of Science, The University of Tokyo, Hongo, Bunkyo-ku, Tokyo 113-0033, Japan.

intensity for single-crystal diffraction experiments in the wavelength range 0.33–0.85 Å, which is ideal for obtaining the high-Q data needed for high real-space resolution. Wavelength selection is made by a Cu(220) monochromator in transmission mode, and appropriate filters are used to remove $\lambda/2$ contamination from the incident neutron beam, which is collimated by the collimation nose. The sample is mounted on a table (the ω table) which rotates it about a vertical axis through an angle ω. The diffracted signal is detected by a two-dimensional area detector, which effectively covers $6 \times 6^\circ$ in 32×32 pixels. In four-circle mode, the detector moves in the horizontal plane about a vertical axis, which is coincident with ω, to access scattering angles (2θ) in the range 5–120°. In normal-beam mode, the detector is additionally able to move −12 to +25° out of the horizontal plane by an angle ν. For alignment, the optical telescope (Fig. 1) is pre-aligned so that its cross hairs are centred on the ω rotation axis at the height of the equatorial plane traced by rotation of the centre of the detector around 2θ and passing through the centre of the monochromator. The incident beam can then be aligned to the diffractometer by centring a test crystal on the ω rotation at the correct height using the telescope, setting the crystal to reflect a strong hkl reflection, and then making small adjustments to the monochromator angle and to the position of the incident-beam-defining apertures (F and G of Fig. 2) until the reflected intensity reaches a maximum.

Under ambient conditions, using wavelengths in the 0.70–0.85 Å range, data collection times of a few minutes per reflection are typical and a full data set can usually be measured in about 2–3 d. However, with the reduced sample size required by the pressure cell, and the significant signal attenuation and reduced access to reciprocal space caused by the sample containment, data collection times are typically increased to 15–20 min per reflection and can become larger still, up to an hour or more, at wavelengths below 0.70 Å. The use of shorter wavelengths not only provides higher real-space resolution but also provides some compensation for the reduction in access to reciprocal space. Measurement of a full, multi-wavelength data set can take of the order of 10 d, and making optimally efficient use of beamtime is an important factor in high-pressure studies.

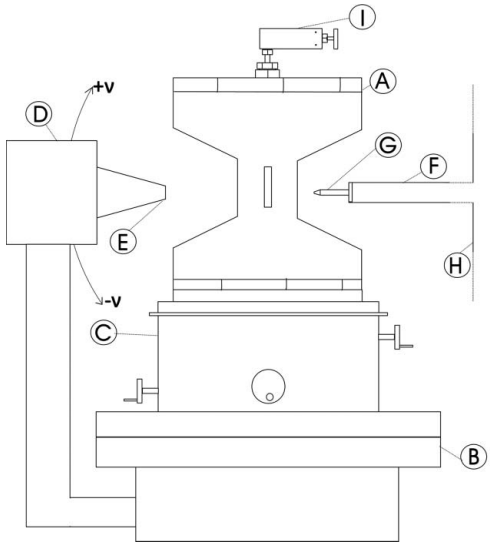

Figure 2
Schematic diagram of the PE VX3 press (labelled A) mounted on the ω table (B) *via* adaptor plates and a Huber XYZ table (C). Also shown are the area detector (D), which can be lifted through an angle $\pm\nu$, and its collimation nose (E), the incident-beam nose (F) with additional incident-beam collimation specific to the PE press (G), and the protective wall (H) behind which is housed the Cu(220) monochromator. The high-pressure oil inlet (I) for the press is also shown.

3. Pressure cells, anvils and sample loading

The VX Paris–Edinburgh (PE) press (Klotz *et al.*, 2004) and its use for single-crystal studies have been described elsewhere in detail (Bull, Guthrie, Nelmes, Loveday, Komatsu *et al.*, 2009; Bull, Guthrie, Nelmes, Loveday, Hamidov & Gutmann, 2009). However, a few key points are worth reiterating. The VX variant of the PE press (shown schematically in Fig. 2) is a two-column press capable of producing up to 250 tonnes (1 tonne = 9.8 kN) of force and providing an increased access to reciprocal space; the load is applied by a hydraulic ram. For the studies set out in this paper, two types of toroidal profile anvils have been used: single toroidal profile anvils made of tungsten carbide (Khvostantsev, 1984; Khvostantsev *et al.*, 2004), with an opening angle of ±20° (Bull *et al.*, 2005), which can reach a maximum pressure of ∼8 GPa; and, for studies above this pressure, single toroidal profile anvils, made of sintered diamond, with an opening angle of ±7° (Besson *et al.*, 1992). To prevent breakage or crushing of the sample crystal on compression, it must be surrounded by a hydrostatic or quasi-hydrostatic medium. For these studies, we have used a modified encapsulated gasket (Marshall & Francis, 2002) machined from a null scattering titanium–zirconium alloy, TiZr (67:33 molar ratio). One-half of the encapsulated gasket is filled with TiZr to provide a flat surface to support the 3–4 mm^3 single crystal (the largest volume a sample can have for 10 GPa studies) and provide a means to maintain the sample orientation upon increasing load. The gasket also encapsulates the surrounding hydrostatic 4:1 deuterated methanol:ethanol mixture (Bull, Guthrie, Nelmes, Loveday, Komatsu *et al.*, 2009).

4. Mounting of the pressure cell

Fig. 2 shows a schematic diagram of the D9 instrument when a VX3 variant PE press (A) has been mounted so that it can rotate around the vertical ω axis of the instrument, and a corresponding picture is shown at the top of Fig. 3. To provide the space needed to mount the press, the offset χ circle has been removed from the ω rotation stage (B). A Huber XYZ table (C) (capable of supporting 150 kg and positioning to ∼1 µm) is mounted on the ω rotation stage, and the 60 kg PE press is mounted on this table using adaptor plates. The ram of the press is at the top, where the high-pressure oil inlet is located (I). The instrument is then used in 'normal-beam' geometry: the area detector is used as a lifting-arm counter (D), which, as said, can move −12 to +25° out of the horizontal

plane through an angle referred to as ν. In data collection, the movement of ν is limited to $\pm 10^\circ$, the range over which emerging diffracted beams pass through only TiZr gasket material, and no anvil material, when using the 20° bevelled anvils designed for lower-pressure studies. This allows accurate attenuation corrections to be made (Bull, Guthrie, Nelmes, Loveday, Komatsu *et al.*, 2009).

5. Alignment of the cell and sample

The sample itself cannot be directly viewed once it is loaded into the press, because the anvils are opaque. Therefore, in order to obtain accurate lattice parameters and integrated intensities, particular effort has to be made to ensure that the sample is placed on the centre of rotation of the instrument at the correct beam height. During loading, care is taken to mount the centre of the cylindrical sample accurately at the centre of the round gasket, itself centred in the anvils, by use of an optical microscope. The anvils and their mounts are designed and machined to ensure that the centre of the gasket coincides with the axis of the PE press, and this procedure ensures that the sample centre is within 0.1 mm of the axis of the press. Once the press has been mounted, a micrometer is fixed to the area detector (D in Fig. 2) and is positioned so that it measures the relative displacement of the PE press as the press is rotated in ω. The displacement can be reduced to less than 0.05 mm by using the XYZ table (C in Fig. 2) to adjust the position of the press in the horizontal plane. To adjust the sample height, a fiducial mark is first placed on the exterior of the gasket at the position of the centre of the sample in the vertical direction, and then the XYZ stage is adjusted in Z to bring the fiducial mark to the height of the cross hairs in the alignment telescope. The sample position is at eye height on the D9 instrument, and hence eye and face guards are used to prevent injury to the operator in the unlikely event of an anvil or gasket failure during alignment.

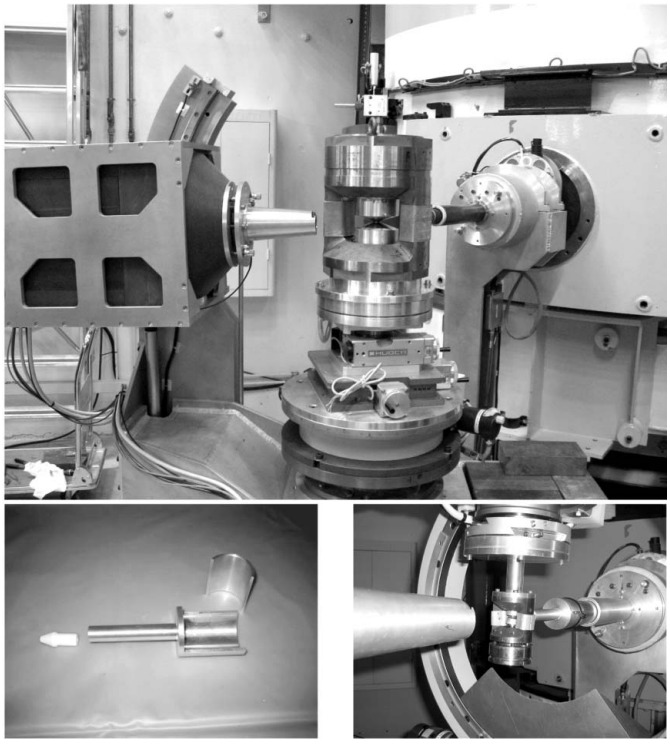

Figure 3
Top: VX3 mounted on the ω table of the D9 instrument. The incident-beam nose can be seen on the right and the area detector to the left. Bottom left: BN collimator and associated aluminium holder (shown detached), the bore of which is lined with B_4C. Bottom right: wide-access panoramic diamond anvil cell mounted on the χ circle of the D9 instrument.

6. Background reduction and collimation

Scattering from the pressure-cell material and gasket surrounding the sample will contribute significantly to the measured scattering. This reduces the peak:background ratio and hence the overall precision of the measurements. To alleviate this problem, effort has been made to reduce the background contribution by development of collimation specific to the PE press. In normal operation, the D9 instrument makes use of a BN disc mounted on the incident-beam nose (F in Fig. 2). For the high-pressure experiments, an additional collimator has been designed to define a smaller beam using an aperture placed much closer to the sample (G in Fig. 2). This collimator consists of an aluminium tube, lined with a 2 mm-thick layer of B_4C, supporting a short piece of BN rod that has a beam-defining aperture machined through its length (shown separated in the lower left of Fig. 3). The BN rod is tapered at its tip to fit between the gap made by the 20° anvils, and can be brought to within 5 mm of the gasket. The size of the aperture through the BN rod is chosen to define as small as possible a beam, consistent with the need to bathe the whole sample in a uniform beam, taking into account any (small) sample movement due to errors in the placing of the sample at the centre of the instrument. These centring errors are normally of the order of 0.2 mm or less. To align the collimator, a selected strong hkl and $\bar{h}\bar{k}\bar{l}$ pair of reflections is first scanned without the collimator to obtain their integrated intensities, and the collimator is then put in place. Both reflections are scanned again, and the alignment of the collimator is adjusted until scans show that both reflections have the same integrated intensity as without the collimator. Once the collimation is in position, with the press mounted on the ω table, as above, or on the χ circle (see later in text for details), care has to be taken to avoid collisions of the collimation with the columns of the press as it is rotated in ω (or in φ if the χ circle is used). Hardware and software limits are put in place to ensure no collisions occur and damage the incident-beam collimation and nose. The collimation has to be removed and realigned each time the press needs to be rotated to measure reflections in a different position of the press's columns.

Fig. 4 shows two-dimensional area detector images of the background close to the 400 reflection of squaric acid (see below) at 5 GPa both without (top left) and with (top right) the additional incident-beam collimation described above, and the difference in background levels is evident. The highest background levels form a band across the image (top left); this

is mainly scattering from the gasket and anvil material, which the additional collimator greatly reduces. The θ–2θ intensity profile scans of the 400 reflection of squaric acid (see below) at 5 GPa in the bottom of Fig. 4 show that the observed level of background is less than half with the collimator nose G (Fig. 2) in place, while the signal strength remains the same. The background-corrected integrated intensity of the reflection is unaltered but its standard deviation is reduced by a factor of three [the integrated intensity of the 400 reflection peak with and without additional collimation is 1097 (15) and 1113 (48), respectively]. This reduction in background becomes even more important when weak reflections are being measured, for example, at high Q, or with smaller samples or at lower incident wavelengths (which have significantly lower fluxes; see later section). The effect of diffracted beam collimation in addition to the normal BN disc aperture on the detector (E in Fig. 2) was also investigated but was found to make no significant reduction in measured background. For this reason, and because it would reduce access to measurable reflections, no additional diffracted beam collimation was used.

7. Reciprocal-space access

Using the techniques described above, it is now possible to obtain accurate high-resolution structural information at pressures up to 10 GPa. Part of this breakthrough is the result of the fact that, although the highest Q measurements (and, hence, highest real-space resolution) can be obtained in the

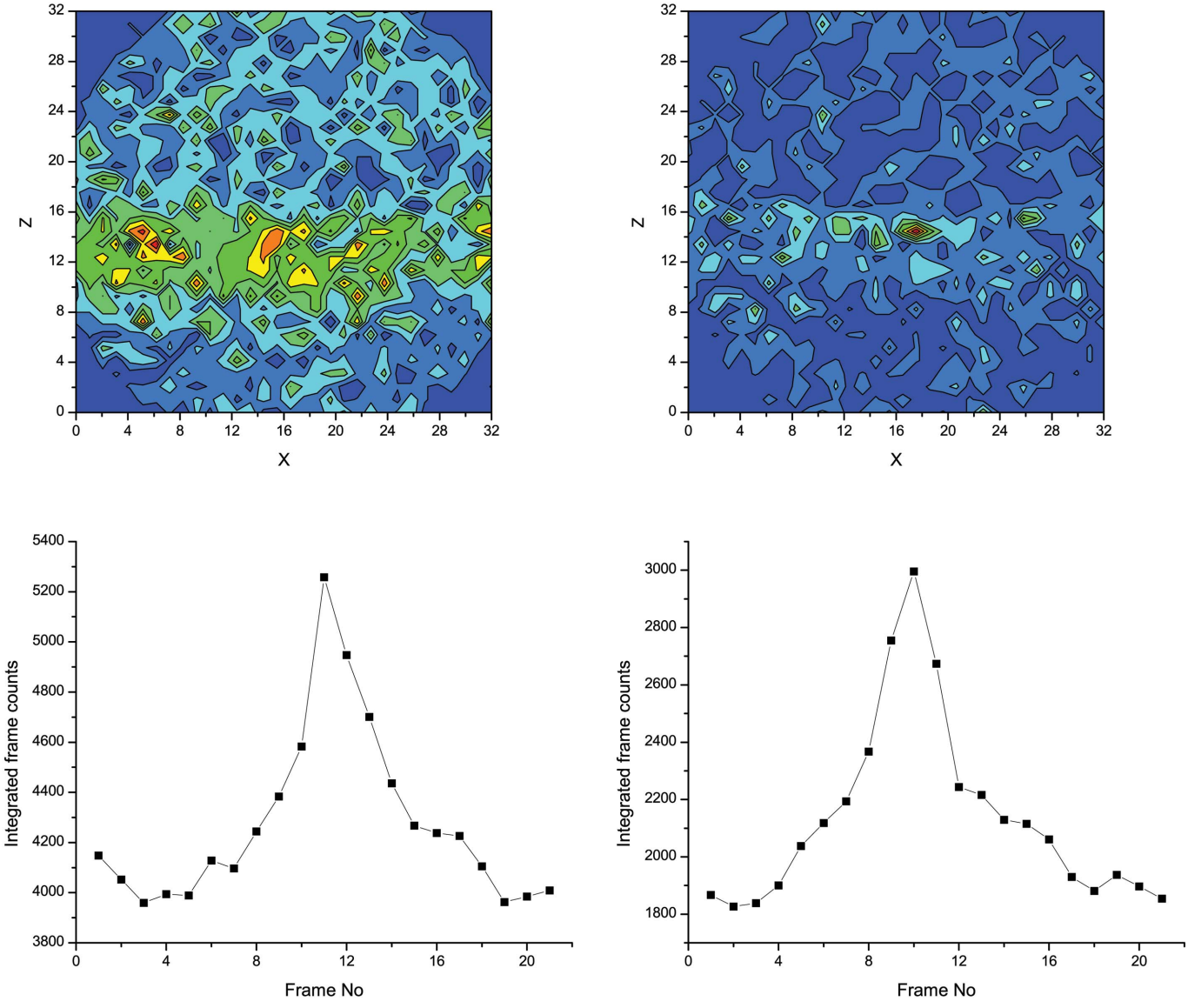

Figure 4
Top: two-dimensional images of the observed background near the 400 reflections of squaric acid at 5 GPa, obtained with the D9 area detector operating in 'normal-beam' (lifting-counter) geometry, (left) recorded without the specially designed incident-beam collimation nose and (right) measured with the collimation nose in place. These images were recorded in frame 1 of the scans shown below the images. Bottom: θ–2θ intensity profile scans are shown (left) without the nose and (right) with the nose for the 400 reflection of squaric acid (see text) at 5 GPa. Note the different 'frame counts' scales in the two profiles. The integrated frame counts are a summation of the counts of all pixels in each frame and each frame is a successive step in the θ–2θ scan.

(horizontal) plane perpendicular to the cell axis, the bevel angle of the anvils allows some access to reciprocal lattice directions out of this plane. The resulting partial three-dimensional character of the data can be crucial to resolving structural features that overlap in strictly two-dimensional data. At pressures below about 8 GPa, where anvils with a 20° bevel angle can be used (Bull *et al.*, 2005), sufficient access out of the horizontal plane can be obtained with wavelengths in the range 0.54–0.84 Å. Above this pressure, anvils with a 7° bevel must be used, and the range of ν for which emerging diffracted beams pass through only gasket material is reduced to less than ±4° for wavelengths of 0.54 Å and greater. For many samples, this restricts the measurement of accurately attenuation-corrected reflection intensities to the equatorial plane. However, the option of using the very short 0.33 Å wavelength available on D9 can bring out-of-plane reflections into the ±4° range of ν for lattice parameters in the vertical direction of 4.7 Å or more. There is a significant loss of incident neutron flux and decreased sample scattering power with lower wavelengths (the maximum of the Maxwellian profile of the hot source at the ILL is centred at 0.84 Å), and hence there is an increase in data collection times. However, even a small number of such measurements can be valuable in resolving structural features that are overlapped in projection onto the horizontal plane. The use of the modified incident-beam collimation (described earlier) becomes even more important at this wavelength because of the much reduced reflection intensities.

8. Structural studies of squaric acid

To date we have determined accurate structure factors from the hydrogen-bonded material squaric acid ($H_2C_4O_4$) up to a pressure of 10 GPa (the limit of methanol–ethanol as a hydrostatic pressure medium at room temperature). The crystal structure (above 0.75 GPa) is tetragonal and has C_4O_4 units, linked by hydrogen bonds, lying in *ab* planes perpendicular to a fourfold axis parallel to the *c* direction of the unit cell (Tun *et al.*, 1987). It had been suggested by high-pressure Raman experiments that the hydrogen bonds centre at 3.5 GPa in this material (Moritomo *et al.*, 1990). We have successfully used the D9 instrument to determine the proton distribution in the hydrogen bonds up to and beyond this proposed transition; the results and interpretation of this study will be reported elsewhere (Bull, Guthrie *et al.*, 2011).

The sample mounting procedures described above allow excellent sample quality to be maintained over the whole pressure range up to 10 GPa, with only a small reduction in sample size, from 4 to 3 mm^3, above ∼7 GPa. The sample crystal was mounted with the *ab* plane of the unit cell horizontal. Fig. 5 shows two-dimensional detector images at the peak maxima of the ω scans through the 400 reflection of squaric acid at ambient pressure and 10 GPa, and the corresponding intensity profiles through the centre of each two-dimensional image. The absence of any change in reflection width indicates that the sample exhibits no detectable damage or strain at 10 GPa.

Table 1
Details of squaric acid high-pressure data collection and structural refinement.†

	3.5 GPa	10 GPa
Number of reflections [$\sigma(I)/I \leq 0.1$]	161	101
Number of independent reflections	61	57
$R_{\rm merge}$ (%)	5.2	3.2
R_1 (%)	4.54	5.19
Goodness of fit (χ^2)	1.445	1.289
Wavelength range used for data collection (Å)	0.71–0.84	0.33–0.71
Crystal size (mm^3)	4	3

† Unlike the goodness of fit, the values of R_1 and $R_{\rm merge}$ apply only to the 0.71 Å data, because of the absence of equivalents for the 0.54 and 0.33 Å data as explained in the text.

A total of 61 independent reflections were measured at 3.5 GPa, out to $\sin\theta/\lambda \simeq 1.0$ Å^{-1}, using a wavelength, λ, of 0.71 Å. Initial sample checking and orientation was carried out at a wavelength of 0.84 Å, near the flux maximum of D9, and then the shorter wavelength was selected to achieve sufficient resolution in determination of the detailed structure. Nearly all reflections in the accessible ∼44% of layers (*hk0*) and (*hk*±1) were measured, including one, and in some cases two, equivalents, and an overall total of 161 reflections were measured with $I \geq 10\sigma(I)$ (Table 1). The $\sin\theta/\lambda$ limit corresponds to limiting indices of $-10 \leq h \leq 11$, $-11 \leq k \leq 11$, for $l = 0$, and $4 \leq h \leq 10$, $3 \leq k \leq 9$, for $l = \pm 1$. The range of only ±1 in *l*, and thus the lack of information in the *c*-axis direction of the structure, is a consequence of the restricted geometry of the pressure cell anvils, as discussed above. However, data measured to high *h* and *k* in the (*hk*0) layer provided high spatial resolution in the two-dimensional layers of the squaric acid structure (Tun *et al.*, 1987), and the ability to measure some reflections with $l = \pm 1$ provided some valuable separation of overlapped *ab* layers, as already discussed. The details in Table 1 show the overall agreement between equivalents ($R_{\rm merge}$) and the quality of fit in the structural refinement (R_1 and goodness of fit) performed using the *SHELX* suite of structure refinement programs (Sheldrick, 2008), where $R_{\rm merge} = \sum_{hkl}\sum_i |F_i(hkl) - F(\bar{h}\bar{k}\bar{l})| / \sum_{hkl}\sum_i |F_i(hkl)|$ and $R_1 = \sum \|F_{\rm o}| - |F_{\rm c}\| / \sum |F_{\rm o}|$.

The data collection at 10 GPa was carried out with a different, slightly smaller, crystal that was oriented the same way, with the *ab* plane of the unit cell horizontal. At this pressure, the access to reflections out of the (*hk*0) plane was more restricted (see above). Data were first collected in the (*hk*0) layer using a wavelength of 0.71 Å to collect approximately the same number of reflections as in the 3.5 GPa data set. The scan through each reflection was made up of 30 frames equally spaced in ω, and the average data collection time per reflection was 15 min. The wavelength was then changed to 0.54 Å to extend the resolution to $\sin\theta/\lambda \simeq 1.5$ Å^{-1}, because of the need to try to resolve structural features, like dimensions in hydrogen bonds, reduced in size by the greater pressure. Because of the considerably greater data collection time caused by the reduction in flux and scattering power at the shorter wavelength, the additional reflections to be measured were selected by using calculations

based on fits to the 0.71 Å data to identify the strongest. Even with this selection, data collection times increased to 50 min per reflection; the number of frames per reflection was kept at 30. In view of the long data collection times, and the evidence, from data already collected, of very good agreement between equivalents (see 3.2% in Table 1), only a single set of independent reflections was measured for this 0.54 Å data set, including a few reflections overlapping with the 0.71 Å set for scaling purposes. To collect any data in the (*hk*1) layer, the wavelength had to be reduced further to 0.33 Å (see above), where reflection intensities are further considerably reduced by loss of flux and scattering power, and the average data collection time per reflection increased to 150 min (with, again, 30 frames per reflection). Leverage procedures (Hazen & Finger, 1989) were used to select nine measurable independent reflections sensitive to the interesting structural dimensions. No equivalents were measured, but two *hk*0 reflections were measured to allow scaling with the other data sets. The total number of independent reflections (Table 1) is slightly smaller than at 3.5 GPa because there was more selection in the data collection (like leverage) and because, although the $\sin\theta/\lambda$ range was greater at 10 GPa, a smaller proportion of reflections had $I \geq 10\sigma(I)$ as a result of factors such as the smaller sample size and the reduced reflection intensities at short wavelengths. In addition, the ratio of total reflections to independent reflections was considerably less than at 3.5 GPa through reduction in the number of equivalents measured. Nevertheless, the goodness of fit – taken over all the data – indicates (Table 1) that the data quality is at least as good as at 3.5 GPa.

At both pressures, the integrated intensities were corrected for the effect of attenuation of the diffracted beams as they pass through the gasket material with path lengths that vary with the angle, ν, of each reflection out of the horizontal plane. Because of the cylindrical symmetry of the gasket about the vertical axis in our loadings, the attenuation correction for the diffracted beam is constant for a given wavelength and angle ν; and the attenuation of the incident beam is the same for all

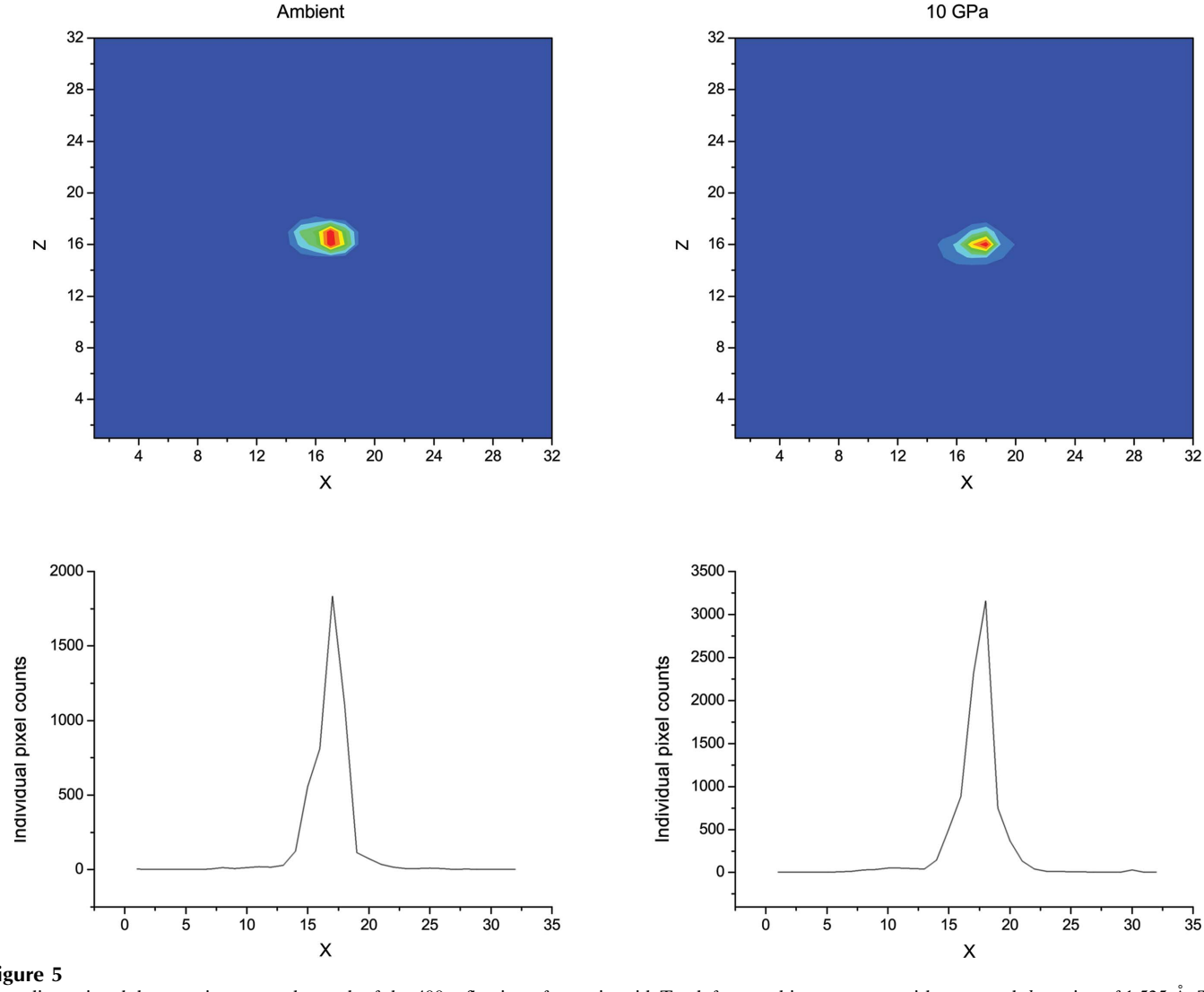

Figure 5
Two-dimensional detector images at the peak of the 400 reflection of squaric acid. Top left: at ambient pressure with a centred *d* spacing of 1.535 Å. Top right: at 10 GPa with a centred *d* spacing of 1.456 Å. Bottom left and right: intensity profiles across the images at $Z = 16$. Note that the background counts are of the order of 2 per pixel, consistent with ∼2000 summed over all pixels as in the profiles shown in Fig. 4.

reflections, both in ($\nu = 0^\circ$) and out of ($\nu \neq 0^\circ$) the equatorial plane. For a given ν, the overall attenuation factor varies linearly with wavelength, from 2.1 at 0.33 Å to 3.3 at 0.84 Å for our equatorial-plane ($\nu = 0^\circ$) data. For diffracted beams out of the equatorial plane, this attenuation factor increases approximately linearly with ν, up to an additional factor of 2.0 at $\nu = 10^\circ$ – so that, for reflections at $\nu = 10^\circ$, the attenuation factor would vary from 4.2 at 0.33 Å to 6.6 at 0.84 Å. The calculation of these factors from the known dimensions of the gasket and anvils has been previously tested by making measurements from the same sample both in and out of the pressure cell (Bull, Guthrie, Nelmes, Loveday, Komatsu *et al.*, 2009). No corrections were required for absorption by the sample itself because of its cylindrical shape.

The results presented in Table 1 and Fig. 5 show that crystal quality and orientation can be maintained up to 10 GPa at least, and that it is possible to collect high-quality high-resolution single-crystal data over the whole range. The data collection at 10 GPa illustrates the kinds of strategy that can be used to optimize the use of experimental time to overcome reduced sample size and angular access at higher pressures.

9. Further developments

Even with just two columns, the VX3 press limits access to reciprocal space, with approximatly 44% of available reflections hidden by the columns of the press for the (*hk*0) plane of a squaric acid crystal oriented so that the *ab* plane is perfectly aligned in the horizontal. To address this, a device capable of rotating the sample and anvil assembly relative to the press, while at load, has been developed and is described in detail elsewhere (Fang *et al.*, 2010). This device allows the sample crystal to be rotated so that regions of reciprocal space obscured by the columns of the press are moved into positions where they can be observed. The motors are fully controlled by the software that drives the existing motors of the D9 instrument and will rotate the crystal to bring specific reflections into the diffraction condition.

We have recently developed the ability to load argon gas at high pressure into the PE press at room temperature to act as a pressure medium, and we have been able to measure single-crystal reflections of sodium chloride and squaric acid up to pressures of 16 GPa under quasi-hydrostatic conditions with no measurable peak broadening (Bocian *et al.*, 2010; Bull, Bocian *et al.*, 2011). This development will increase further the scope of science that it is possible to perform on the D9 instrument.

We are also developing the use of gem-anvil cells to make it possible to use neutron-diffraction techniques to study single crystals of materials that are liquids or gases under ambient conditions. The Ahsbahs sapphire anvil cell has been successfully used in this way on D9 at pressures up to ~1 GPa with a sample of ice VI, and has been described elsewhere (Kuhs *et al.*, 1989). We have now been making efforts to mount the small VX1 variant of the PE press on the χ circle for work with similar samples using diamond gem anvils. These permit direct visual observation of *in situ* grown samples and direct determination of the sample pressure by spectroscopic measurement. The mass of the VX1 press is ~10 kg and it is capable of producing 50 tonnes of force (Klotz *et al.*, 2004). The two columns provide two apertures of 140° each in the equatorial plane and up to 60° out of plane (±30°), but the usable out-of-plane range is ultimately limited by the dimensions and geometry of the anvils and associated tungsten carbide supports. The VX1 press has been successfully mounted and used on the χ circle of D9 (Fig. 3), but its mass limits the χ angle that can be used to ±10° from the bottom of the circle. We have also mounted a clamped wide-access panoramic diamond anvil cell (Mao *et al.*, 2001) with a similar angular access. However, the cell has a mass of only ~0.75 kg, at the expense of load capability, and the reduced mass allows full angular use of the χ circle (Fig. 3). Reflections from samples of ice VI grown *in situ* at high pressure in both cells have been successfully measured using the χ circle.

However, success in working with *in situ* grown crystals has been limited by difficulties in transporting loaded pressure cells from the UK to the ILL. Loadings are often not sufficiently stable to survive the disturbances of travel, particularly as the pressure increases above ~2 GPa. For example, recent attempts to collect data from crystals of ammonia hydrate grown at 3 GPa were thwarted by loss of several samples in transit until one crystal did survive the journey and then a good data set of 147 reflections was obtained. There is thus a need to have improved facilities to load and grow such samples at the ILL. We are currently working with the ILL and ESRF to establish suitable support laboratories for these purposes.

10. Conclusions

In summary, recent developments in pressure technology now allow single-crystal samples of a size suitable for neutron scattering experiments to be compressed to 10 GPa, with further progress to 16 GPa now in prospect. We have now combined this technological advance with the unique capabilities of the D9 diffractometer at the ILL to obtain high-resolution structural information at high pressure. Specially developed collimation to minimize structured background scattering from the pressure-cell materials and the use of area detectors to discriminate between signal and background scattering are crucial. The ability to tune the incident neutron wavelength on D9 over a range, down to very short wavelengths, and combine multi-wavelength data sets allows use of measurement time to be optimized, with shorter lower-flux wavelengths used only for selected high-index reflections. The use of leverage techniques in selecting reflections is a key part of this strategy. So also is the use of accurately cylindrical samples (and gaskets) to reduce the need to measure equivalent reflections. Taken together these advances open up a wide range of new scientific opportunities, including the study of multi-site disorder, anharmonicity and accurate measurements of anisotropic thermal motion at high pressure.

We gratefully acknowledge the scientific and technical advice of Stefan Klotz (UPMC) and John Allibon (ILL). This

work was funded by the Engineering and Physical Sciences Research Council and supported through resources and beamtime made available by the Science and Technology Facilities Council and by the ILL.

References

Besson, J. M., Nelmes, R. J., Hamel, G., Loveday, J. S., Weill, G. & Hull, S. (1992). *Physica B*, **180**, 907–910.
Bocian, A., Bull, C. L., Hamidov, H., Loveday, J. S., Loveday, R. J. & Kamenev, K. V. (2010). *Rev. Sci. Instrum.* **81**, 093904.
Bull, C. L., Bocian, A., Hamidov, H., Kamenev, K. V., Loveday, J. S. & Nelmes, R. J. (2011). *Rev. Sci. Instrum.* **82**, 076101.
Bull, C. L., Guthrie, M., Klotz, S., Philippe, J., Strässle, T., Nelmes, R. J., Loveday, J. S. & Hamel, G. (2005). *High Press. Res.* **25**, 229–233.
Bull, C. L., Guthrie, M., Nelmes, R. J., Loveday, J. S., Hamidov, H. & Gutmann, M. J. (2009). *High Press. Res.* **29**, 644–648.
Bull, C. L., Guthrie, M., Nelmes, R. J., Loveday, J. S., Komatsu, K. & Fernandez-Diaz, M. T. (2011). *J. Chem. Phys.* Submitted.
Bull, C. L., Guthrie, M., Nelmes, R. J., Loveday, J. S., Komatsu, K., Hamidov, H. & Gutmann, M. J. (2009). *High Press. Res.* **29**, 780–791.
Fang, J., Bull, C. L., Hamidov, H., Loveday, J. S., Gutmann, M. J., Nelmes, R. J. & Kamanev, K. V. (2010). *Rev. Sci. Instrum.* **81**, 113901.
Hazen, R. M. & Finger, L. W. (1989). *Am. Mineral.* **74**, 352–359.
Khvostantsev, L. G. (1984). *High Temp. High Press.* **16**, 165.
Khvostantsev, L. G., Slesarev, V. N. & Brazhkin, V. V. (2004). *High Press. Res.* **24**, 371–383.
Klotz, S., Hamel, G. & Frelat, J. (2004). *High Press. Res.* **24**, 219–223.
Kuhs, W. F., Ahsbahs, H., Londono, D. & Finney, J. L. (1989). *Physica B*, **156**, 684–687.
Mao, H. K. *et al.* (2001). *Science*, **292**, 914–916.
Marshall, W. G. & Francis, D. J. (2002). *J. Appl. Cryst.* **35**, 122–125.
McMahon, M. I., Nelmes, R. J., Kuhs, W. F. & Piltz, R. O. (1990). *Europhys. Lett.* **13**, 143–148.
Moritomo, Y., Koshihara, S. & Tokura, Y. (1990). *J. Chem. Phys.* **93**, 5429–5435.
Nelmes, R. J., Tun, Z. & Kuhs, W. F. (1987). *Ferroelectrics*, **71**, 125–141.
Sheldrick, G. M. (2008). *Acta Cryst.* A**64**, 112–122.
Tun, Z., Nelmes, R. J. & McIntyre, G. J. (1987). *J. Phys. C*, **20**, 5667–5675.